FEBS Letters

FEBS PRESS science publishing by scientists

Non-Debye frustrated hydration steers biomolecular association: interfacial tension for the drug designer

Ariel Fernández[1,2]

1 Argentine Mathematics Institute (I. A. M.), National Research Council (CONICET), Buenos Aires, Argentina
2 AF Innovation, Pharmaceutical Consultancy GmbH, Buenos Aires, Argentina

Correspondence
A. Fernández, Argentine Mathematics Institute (I. A. M.), National Research Council (CONICET), Buenos Aires 1083, Argentina
Fax/Tel: 54 11 4954 6781
E-mail: ariel@afinnovation.com

(Received 27 June 2016, revised 30 August 2016, accepted 31 August 2016, available online 2 October 2016)

doi:10.1002/1873-3468.12418

Edited by Alfonso Valencia

Many cellular functions involve the assembly of biomolecular complexes, a process mediated by water that gets displaced as subunits bind. This process affects water frustration, that is, the number of unmet hydrogen-bonding opportunities at the protein–water interface. By searching for least-frustrated aqueous interfaces, this study delineates the role of frustration in steering molecular assemblage. The search entails a trajectory sampling using a functional that measures the gradient of frustration and computing the resulting non-Debye electrostatics within relaxation times for coupled protein–water systems. The minimal frustration principle is validated against spectroscopic measurements of frustration-dependent dielectric relaxation, affinity scanning of protein–protein interfaces, and NMR-inferred association propensities of protein-complex intermediates. The methods are applied to drug design, revealing the targetable nature of the aqueous interface.

Keywords: aqueous interface; drug design; molecular modeling; protein associations; structural biology

With the recognition that no cogent theory fully reconciles thermodynamic and structural characterization of protein associations, and that hydrophobicity is hardly operative at Angstrom-level curvatures, the forces that steer the formation of protein complexes remain under intense scrutiny [1–6]. This work addresses this problem, investigating protein-complex formation from a solvent-centric perspective that takes into account the unusual properties of water near biomolecular surfaces. The approach requires a variational procedure to optimize the frustration state [7] of the aqueous interface. Frustration refers to the unmet opportunities for hydrogen-bonding that cause interfacial tension [6]. It is at present unclear whether force fields and solvation models adopted in molecular dynamics (MD) computations can properly model frustration or capture interfacial tension [8–12]. It is also unclear—and unlikely—that the global free-energy minimum would be a state of minimal interfacial frustration and, while the biological relevance of the former is still debated, the latter is clearly decisive in driving complex formation, as this work shows [5,11].

As shown in this work, a special microstate sampling strategy steering MD computations toward the least-frustrated interface proves essential to identify the molecular factors that trigger complexation. Accordingly, we implement and experimentally validate an explicit-solvent MD algorithm with microstate sampling guided by a functional that defines a variational principle to enable the search for minimally frustrated interfaces. The functional form of the variational principle hinges on the *ansatz* that frustration creates a polarization component decoupled from the electrostatic field [5,6]. The functional adopted exploits

Abbreviations
hGH, human growth hormone; MD, molecular dynamics; PDB, protein data bank; PI3K, phosphoinositide 3-kinase; PP, protein–protein; PTEN, phosphatase and tensin homolog.

the link between frustration and electrostatics and computes the non-Debye electrostatic energy equivalently stored as the frustration-related interfacial tension [5]. Experimental evidence supports this assumption, as shown in the Appendix S1. Thus, the trajectories generated entail the computation of the gradient of frustration at each spatial location.

We demonstrate that frustration-related water polarization steers protein–protein (PP) associations with high specificity and drives the dynamics of complex formation. The validation of these assertions entails contrasting optimally frustrated states with affinity scanning of PP-interfaces [13] in complexes that assemble to mitigate frustrated hydration of free subunits, and with NMR information on the dynamics of complex formation [14]. Subsequently, we identify the optimal sequence of steps that maximize the mitigation of interfacial tension, funneling complex formation. Finally, we apply the solvent-centric approach to drug design in order to demonstrate the efficacy of the variational approach to engineer ultraspecificity, creating ligands that discriminate isoforms of target proteins.

Methods

All operating concepts, equations and symbols are introduced and described in the next section.

Computing the least-frustrated interface

The least-frustrated state of the aqueous interface is represented by an extremal frustration field ϕ that satisfies the Euler-Lagrange equation [15]:

$$\nabla\partial\frac{\mathcal{L}(\phi)}{\partial\nabla\phi}=\partial\frac{\mathcal{L}(\phi)}{\partial\phi}, \tag{1}$$

written explicitly as

$$\nabla^2\phi=\left(\frac{k_BT}{4\omega}\right)(\rho_0-\rho)\left(1-\frac{\phi}{4}\right)^{-1}. \tag{2}$$

Equation (2) constitutes the fundamental relation controlling water frustration at protein interfaces. For small frustration $0<\phi\ll4$, the linear approximation $dS_{if}(\phi)\approx-[k_B(\rho_0-\rho)(\phi/4)]d\vec{r}$ yields the simplified equation $\nabla^2\phi=((k_BT)/4\omega)(\rho_0-\rho)$.

As shown in Appendix S1, to obtain ω, we use Eqn (5) applied to an equilibrating computation of ϕ obtained as a function of the distance X to a rigid nonpolar interface [6,16] consisting of a concave region of fixed curvature radius. The equilibration is carried out for 1 ns, a time incommensurably larger than the relaxation timescale for the decoupled water lattice (~ 1 ps) [17]. Thus, at $T = 298$ K, Eqn (5) yields $\omega=9.18\times10^{-20}\text{mJ}\text{Å}^{-1}$, an estimation validated by contrasting it with the Young-Laplace computation of interfacial free energy [18].

Microstate sampling strategy to steer the search for the least-frustrated state

As shown in the microstate sampling scheme in Fig. 1, we can select at each stage of the simulation a representative from the set of *a priori* equiprobable microstates to ensure a *probable* decrease in $\Delta G_{if}(\phi)=\Im(\phi)$, thus steering the search toward a state of minimal frustration. Let $[\mathbf{Q_n}, \mathbf{P_n}]$ denote the state of the system at stage n, specified by $\mathbf{Q_n}=\mathbf{Q_n^p}\oplus\mathbf{Q_n^w}$ = atomic coordinates vector, and $\mathbf{P_n}=\mathbf{P_n^p}\oplus\mathbf{P_n^w}$ = momentum vector, both decomposable as direct sums of protein (p) and water (w) contributions. The next state $[\mathbf{Q_{n+1}},\mathbf{P_{n+1}^p}\oplus\mathbf{P_{n+1}^w}]$ resulting after 5 ps of MD simulation is retained depending on a comparison of the scalar fields $\phi_n=\phi_n(\mathbf{Q_n})$ and $\phi_{n+1}=\phi_{n+1}(\mathbf{Q_{n+1}})$. State $[\mathbf{Q_{n+1}},\ \mathbf{P_{n+1}^p}\oplus\mathbf{P_{n+1}^w}]$ is retained provided that either one of the following conditions holds:

$$\Im(\phi_{n+1})\le\Im(\phi_n),$$

$$\Im(\phi_{n+1})>\Im(\phi_n)\,\text{and}\,r\le\exp\{-\beta[\Im(\phi_{n+1})-\Im(\phi_n)]\}$$

with r = realization value of random variable adopting real values in the interval [0, 1] and $\beta=[k_BT]^{-1}$. If $\Im(\phi_{n+1})>\Im(\phi_n)\,\text{and}\,r>\exp\{-\beta[\Im(\phi_{n+1})-\Im(\phi_n)]\}$, we perform 5 ps MD runs on 1000 initial randomly selected *a priori* equiprobable microstates $[\mathbf{Q_n},\mathbf{P_n^p}\oplus\mathbf{P_n^{w(j)}}],\text{j}=1,2,\ldots,1000$, with randomly chosen water momenta $\mathbf{P_n^{w(j)}}(\mathbf{P_n^{w(1)}}=\mathbf{P_n^w})$ subject to the constant kinetic energy constraint, and select the state $[\mathbf{Q_{n+1}^*},\mathbf{P_{n+1}^{p*}}\oplus\mathbf{P_{n+1}^{w*}}]$ as the $(n+1)$-destiny state that realizes the lowest value $\Im(\phi_{n+1}(\mathbf{Q_{n+1}^{(j)}}))$.

Identification of packing defects in proteins

To identify packing defects (dehydrons) in soluble proteins, a dehydron calculator may be used. One such calculator that uses structural PDB coordinates as input is obtained as a PYMOL plugin and has been deposited in the PYMOL script repository at the url: https://github.com/Pymol-Scripts/Pymol-script-repo/blob/master/plugins/dehydron.py.

Results

Water configurations with minimal frustration

To describe locally frustrated hydration, we introduce a 'frustration scalar field' $\phi=\phi(\mathbf{r})$ that indicates the

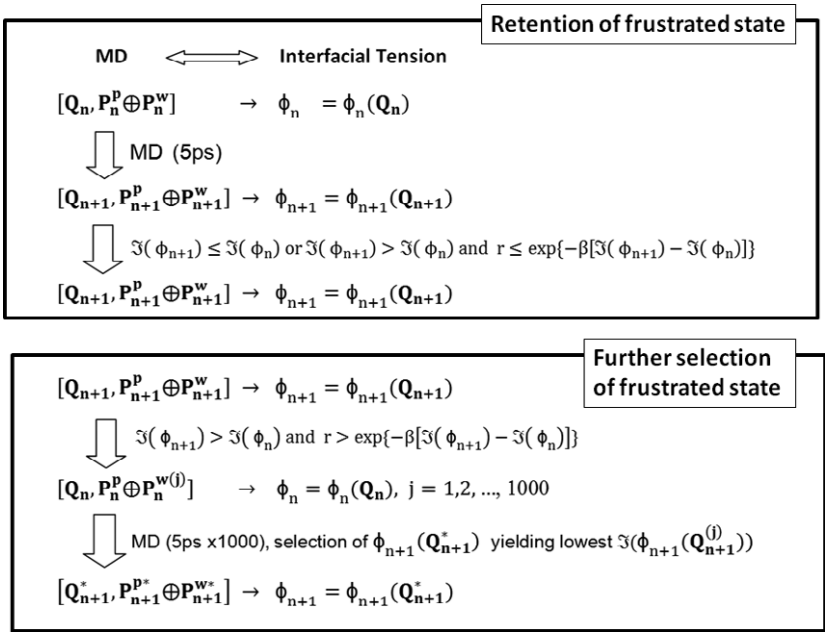

Fig. 1. Scheme of microstate sampling strategy to steer the search toward the state of minimal frustration. Retention or further selection step for a 5 ps-MD iteration controlled by interfacial frustration functional $\Im(\phi)$. The upper box indicates flow under which the destiny microstate $[\mathbf{Q_{n+1}}, \mathbf{P_{n+1}^p} \oplus \mathbf{P_{n+1}^w}]$ is retained in the $n \rightarrow n+1$ iteration based on a comparison of scalar fields $\phi_n = \phi_n(\mathbf{Q_n})$ and $\phi_{n+1} = \phi_{n+1}(\mathbf{Q_{n+1}})$. The lower box indicates the sampling procedure that takes place when the destiny state is not retained and further exploration is required.

expected number of missed hydrogen bond opportunities of a test water molecule at spatial location **r** relative to the quasi-tetrahedral coordination associated with bulk water. The frustration field is defined as $\phi(\mathbf{r}) = 4 - g(\mathbf{r})$, where $g(\mathbf{r}) \leq 4$ is the time-averaged number of hydrogen bonds engaging a water molecule visiting a sphere of radius $r = 4$ Å centered at position **r** for a minimum time period $\tau = 1$ ps, a permanence time typically associated with the relaxation timescale for a decoupled water lattice [17]. The hydrogen bond is operationally defined via geometric constraints [5,12]: O–O distance < 3.2 Å and O–H–O angle α_{HB} satisfying $120° \leq \alpha_{HB} \leq 180°$.

Water frustration is caused by partial nanoscale confinement at the protein surface and hence introduces a component $\overrightarrow{P^{\#}}$ of the polarization vector $\vec{P}$ that is uncoupled from the electrostatic field $\vec{E}$ and orthogonal to the Debye polarization component $\overrightarrow{P^{\parallel}}$ [5,6]. Thus, the interfacial energy is stored in the electrostatic energy term

$$\Delta U^{\#} = \frac{1}{2}\varepsilon_0^{-1}\int ||\overrightarrow{P^{\#}}||^2 \mathrm{d}\vec{r} = \frac{1}{2}\int \omega||\vec{\nabla}\phi||^2 \mathrm{d}\vec{r} \quad (3)$$

where the elastic integral on the r.h.s. results from the *ansatz* [5]:

$$\overrightarrow{P^{\#}} = -\xi\nabla\phi, \quad \xi = (\omega\varepsilon_0)^{1/2} \quad (4)$$

pointing to water frustration, with its lack of partial charge cancellation, as causative of the anomalous non-Debye polarization. The conceptual link between frustration and non-Debye electrostatics defined by Eqn (4) is experimentally validated as shown in Appendix S1, where the prior determination of the constant ω is also provided. Equation (4) implies that the non-Debye electrostatic energy may be equivalently stored as interfacial tension, which is frustration-related [5]. Thus, the link between frustration and electrostatics combined with a standard entropic model used in the derivation of a Poisson-Boltzmann equation [19] motivates the choice of a Lagrangian $\mathcal{L}(\phi)$ defining a free-energy functional $\Im(\phi) = \int \mathcal{L}(\phi)\mathrm{d}\vec{r}$. This functional is thus introduced to compute the free-energy cost $\Delta G_{if}(\phi)$ of generating the water frustration field ϕ when spanning an aqueous interface enveloping the solute:

$$\Delta G_{if}(\phi) = \Im(\phi) = \int \left[\frac{1}{2}\omega||\vec{\nabla}\phi||^2 - k_B T(\rho_0 - \rho)\ln\left(1 - \frac{\phi}{4}\right)\right]\mathrm{d}\vec{r}. \quad (5)$$

The elastic energy term $\int 1/2\omega||\vec{\nabla}\phi||^2\mathrm{d}\vec{r}$ from Eqn (3) is a Dirichlet-type functional [12,15] penalizing departures from bulk structure, and the interfacial entropy differential $\mathrm{d}S_{if}(\phi) = k_B \ln[(4-\phi)/4]^{(\rho_0-\rho)\mathrm{d}\vec{r}} = [k_B(\rho_0 - \rho)\ln(1 - (\phi/4))]\mathrm{d}\vec{r}$ corresponds to the transference of a water molecule from bulk solvent (number density $\rho_0 = 0.033$ Å^{-3}) to a differential volume region $\mathrm{d}\vec{r}$ located at position **r** with number density $\rho(\mathbf{r})$ and frustration $\phi = \phi(\mathbf{r})$. For small structural distortions at $0 < \phi \ll 4$, a linear approximation yields $\mathrm{d}S_{if}(\phi) \approx -[k_B(\rho_0 - \rho)(\phi/4)]\mathrm{d}\vec{r}$.

The least-frustrated state of the aqueous interface is represented by an extremal frustration field ϕ

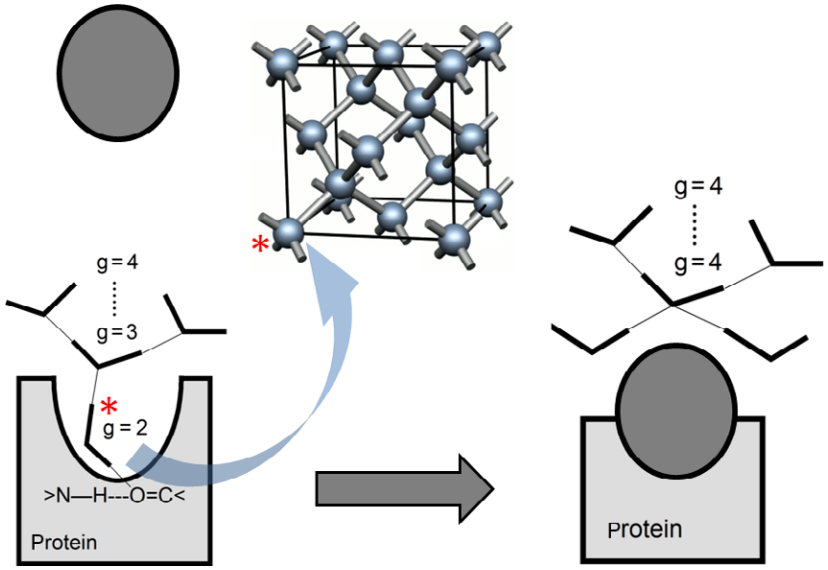

Fig. 2. Scheme of frustrated hydration funneling protein association: A solvent-exposed backbone hydrogen bond, known as *dehydron* [5,6], constitutes a packing defect that generates frustration at the interface ($g < 4$) as a water molecule hydrogen bonds to the backbone carbonyl (exploiting the lone an unused electron pair in the carbonyl oxygen) and thus gets confined in the dehydron cavity. The reader is reminded that the carbonyl oxygen is a double proton acceptor because of its two lone electron pairs in the outer shell orbitals. The transference of the frustrated molecule (marked by the asterisk) to the bulk quasi-tetrahedral lattice of hydrogen bonds is thermodynamically favored and prompts the PP association as an expedient to reduce the interfacial tension.

determined as described in the Methods section. The minimization of interfacial frustration is shown to translate into a major factor steering protein associations (Fig. 2). Frustration cannot be incorporated explicitly into the canonical-ensemble molecular dynamics of soluble proteins since there is no energetic penalty for missed interactions. Yet, as shown in Methods section, we can select at each stage of the simulation a representative from the set of *a priori* equiprobable microstates to ensure a *likely* decrease in $\Delta G_{if}(\phi) = \Im(\phi)$ that would ultimately lead to an effective search for a state of minimal frustration.

Maximal reduction of water frustration steers highly specific protein–protein associations

To assess the steering power of the functional given in Eqn (5) toward the minimally frustrated interfacial state, and illustrate the role of frustrated hydration as promoter of protein associations, we generated 500 ps-trajectories for soluble proteins known to engage in complexes with structures reported in the protein data bank (PDB). A TIP3P explicit solvent [20] within an AMBER package [21,22] and Coulombic interactions evaluated with the Ewald summation scheme [23] were

Fig. 3. Water frustration as steer of protein associations probed by alanine scanning: (A) Steering power of microstate sampling defined by the functional in Eqn (5) (Methods). The search for the minimally frustrated interface state is evidenced by the time evolution of $\Delta G_{if}(\phi) = \Im(\phi)$ during 500 ps-MD trajectories. The single trajectory is in solid thin line, the average over 20 trajectories in thick gray line, while the dashed gray line represents an average over 20 control 500 ps-trajectories with no microstate sampling. Initial structural coordinates were obtained for the corresponding hGHbp receptor chain in the free state that forms a 1 : 1 complex with the human growth hormone (hGH) (PDB 3HHR). The minimal $\Delta G_{if}(\phi)$-value is reached within the 350–400 ps range. (B) Correlation ($R^2 = 0.88$) between $-\Delta\Delta G_{if}$ and $\Delta\Delta G_a$ for site-directed mutational substitution of interfacial residues in hGHbp, yielding the approximate relation $-\Delta\Delta G_{if} \approx \Delta\Delta G_a$. (C) Interfacial tension reduction in the MDM2-p53-transactivation domain complex (PDB 1YCR). Hot spots are identified as preformed backbone hydrogen bonds exposed to water (dehydrons) in the free p53 subunit, undergoing displacement of vicinal water upon association. The displacement results from the approach of a side chain of the binding partner and is marked by a thin line from the α-carbon of the displacing side chain to the center of the dehydron. The dehydrons from the MDM2 peptide are induced upon binding. Hydrogen bonds are represented as lines joining paired residues in a virtual-bond-α-carbon representation. The ribbon rendering on the right is an aid to the eye. (D) Displacement by MDM2 residue L26 of frustrated water around preformed hot-spot dehydrons in the p53-transactivation domain upon association. (E) Residue classification for PDB-reported protein complexes with available affinity scanning data according to $\Delta\Delta G_a$-values and $-\Delta\Delta G_{if}$-values. In the upper row for each PP interface, the classification is established according to the ranges $\Delta\Delta G_a \geq 3$ kcal·mol^{-1} (red), 1 kcal·mol$^{-1} \leq \Delta\Delta G_a < 3$ kcal·mol^{-1} (white), and $\Delta\Delta G_a < 1$ kcal·mol^{-1} (blue). In the lower row residues are labeled following the second classifier ($-\Delta\Delta G_{if}$), according to the ranges $-\Delta\Delta G_{if} \geq 3$ kcal·mol^{-1} (red), 1 kcal·mol$^{-1} \leq -\Delta\Delta G_{if} < 3$ kcal·mol^{-1} (white), and $-\Delta\Delta G_{if} < 1$ kcal·mol^{-1} (blue).

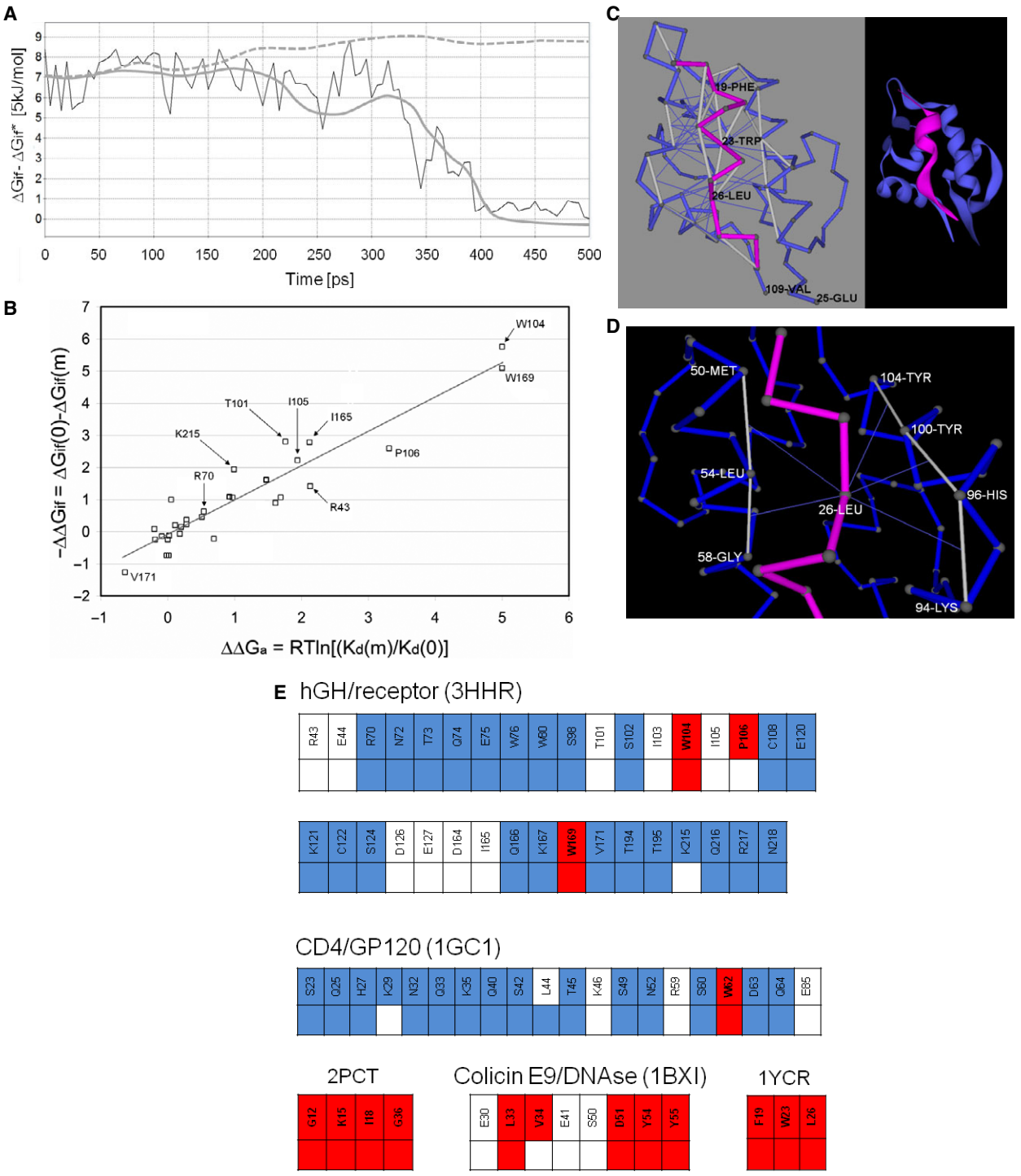

adopted for MD simulation steered by the microstate sampling strategy described in Methods. An isothermal/isobaric ensemble at $T = 298$ K was adopted with initial structural coordinates for the protein chain obtained for the corresponding free subunit extracted *in silico* from the PDB-reported complex. The free (uncomplexed) protein subunits were solvated in a water box extending at least 10 Å beyond any protein atom and were thermalized for 5 ns [24]. Following relaxation, positional restraints defined by force

constant = 5 kcal·Å^{-2} were imposed on all protein non-hydrogen atoms.

In Fig. 3A, we report the time evolution of $\Delta G_{if}(\phi) = \Im(\phi)$ for the free human growth hormone (hGH) receptor subunit hGHbp that forms the receptor/hGH complex, adopting the structural coordinates for the individual subunits provided in PDB entry 3HHR [13] with the structures thermalized as previously indicated. The thin solid line reports a single trajectory, the thick solid gray line, the average over 20 trajectories following the iterative scheme given in Methods, and the dashed line represents the control consisting of an average over 20 trajectories of 500 ps-MD simulation without enforcing the microstate sampling strategy. The minimal $\Delta G_{if}(\phi)$-value is $\Delta G^{*}_{if}(\phi) = 121\,\mathrm{kJ\cdot mol^{-1}}$, corresponding to interfacial tension $\gamma = 2.13\ \mathrm{mJ\cdot m^{-2}}$. A significant relaxation is observed in the 350–400 ps range (Fig. 3A), in agreement with experimental relaxation times for the coupling of protein motion and hydration pattern [23]. It should be noted that such values are incommensurably larger than the relaxation time for the decoupled water lattice (~ 1 ps) previously incorporated [17].

To assert the role of interfacial water frustration as promoter of PP association (cf. Fig. 2), we determine the effect of site-directed mutations on the interfacial free-energy increment $\Delta G_{if}(\phi)$, and compare the $\Delta\Delta G_{if}(\phi)$ values with the change in affinity quantified by the calorimetrically measured $\Delta\Delta G_a = RT\ \ln[(K_d(m))/(K_d(0))]$, where $\Delta\Delta G_a$ is the change in association free energy that results from a site-specific mutation [13], with $K_d(m)$, $K_d(0)$ indicating the equilibrium dissociation constants for mutant (m) and wild-type (0), respectively. Hot spots in PP associations were experimentally identified by alanine scanning of the PP interface [13]. This technique involves site-specific amino acid substitution for alanine (effectively, a side-chain truncation). The most comprehensively scanned interface corresponds to the 1 : 1 hGH-hGHbp complex [13]. Thus, the changes in affinity measured by $\Delta\Delta G_a$ and obtained from alanine scanning were contrasted with *in silico* substitution effects computed as changes in interfacial free-energy $\Delta\Delta G_{if} = \Delta G_{if}(m) - \Delta G_{if}(0)$. A tight correlation ($R^2 = 0.88$) between $-\Delta\Delta G_{if}$ and $\Delta\Delta G_a$ corresponding to the scanning of the receptor hGHbp (Fig. 3B), supports the relation $-\Delta\Delta G_{if} \approx \Delta\Delta G_a$, and upholds the view that the complexes assemble to reduce the interfacial tension of the free subunits.

To further support this assertion, other protein associations were considered where $\Delta\Delta G_a$-values were available [13,25–28]. For example, the p53 transactivation domain, that forms a complex with MDM2 (PDB 1YCR) [28], has been thermalized and equilibrated in free form following the protocol previously indicated to identify hot spots representing contributions $\geq 3\ \mathrm{kcal\cdot mol^{-1}}$ to ΔG_{if}. Such hot spots correspond to the frustrated water partially confined in the cavities formed by packing defects in the protein structure (Fig. 2) [5,6]. These defects consist of solvent-exposed backbone hydrogen bonds, known as *dehydrons* (Fig. 3C). The backbone hydrogen bonds in the MDM2 fragment are induced upon binding and do not constitute hot spots, since no stable structure can be sustained by the MDM2 peptide in free form. Upon forming the complex, residues F19, W23, and L26 in MDM2 have been identified as removing frustrated water from the vicinity of the hot-spot p53 dehydrons shown in Fig. 3C. For example, L26 displaces frustrated water from hot-spot dehydrons M50-L54, L54-G58, L94-H96, H96-Y100, and Y100-Y104, as shown in Fig. 3D. These considerations lead us to identify MDM2 residues F19, W23, and L26 as the significant contributors, yielding $-\Delta\Delta G_{if} \geq 3\ \mathrm{kcal\cdot mol^{-1}}$ upon *in silico* scanning of the PP interface. This result is in accord with the experimental alanine scanning yielding $\Delta\Delta G_a \geq 3\ \mathrm{kcal\cdot mol^{-1}}$ solely for these three residues in MDM2 [28].

To extend and simplify the analysis, we classified residues according to $\Delta\Delta G_a$-ranges and independently according to $\Delta\Delta G_{if}$-ranges. Adopting the affinity classifier, hot-spot residues are labeled (upper row for each PP interface, Fig. 3E) according to the ranges $\Delta\Delta G_a \geq 3\ \mathrm{kcal\cdot mol^{-1}}$ (red), $1\ \mathrm{kcal\cdot mol^{-1}} \leq \Delta\Delta G_a < 3\ \mathrm{kcal\cdot mol^{-1}}$ (white), and $\Delta\Delta G_a < 1\ \mathrm{kcal\cdot mol^{-1}}$ (blue). Adopting the interfacial tension classifier (lower row for each PP interface), residues are labeled according to the ranges $-\Delta\Delta G_{if} \geq 3\ \mathrm{kcal\cdot mol^{-1}}$ (red), $1\ \mathrm{kcal\cdot mol^{-1}} \leq -\Delta\Delta G_{if} < 3\ \mathrm{kcal\cdot mol^{-1}}$ (white), and $-\Delta\Delta G_{if} < 1\ \mathrm{kcal\cdot mol^{-1}}$ (blue). Using these two classifiers, the PP interfaces for five complexes with scanning data available were examined: hGH/hGHbp receptor (3HHR) [13], HIV-1-CD4/GP120 (1GC1) [25], trypsin inhibitor/beta-trypsin (2PTC) [26], colicin E9 immuno-protein/colicin E9 DNase domain (1BXI) [27] and p53/MDM2 (1YCR) [28]. The significant correlation between the $\Delta\Delta G_a$ and $-\Delta\Delta G_{if}$ classifiers (Fig. 3E, P-value < 10^{-5}) upholds the view that interfacial tension generated by frustrated hydration drives protein association.

Interfacial frustration and association propensity in complex-denaturation intermediates

To further validate the variational frustration principle we analyze the complex dissociation intermediates arising from progressive cold denaturation of homodimeric repressor protein CgIR2, a system for which the dynamic intermediates have been resolved at atomic resolution

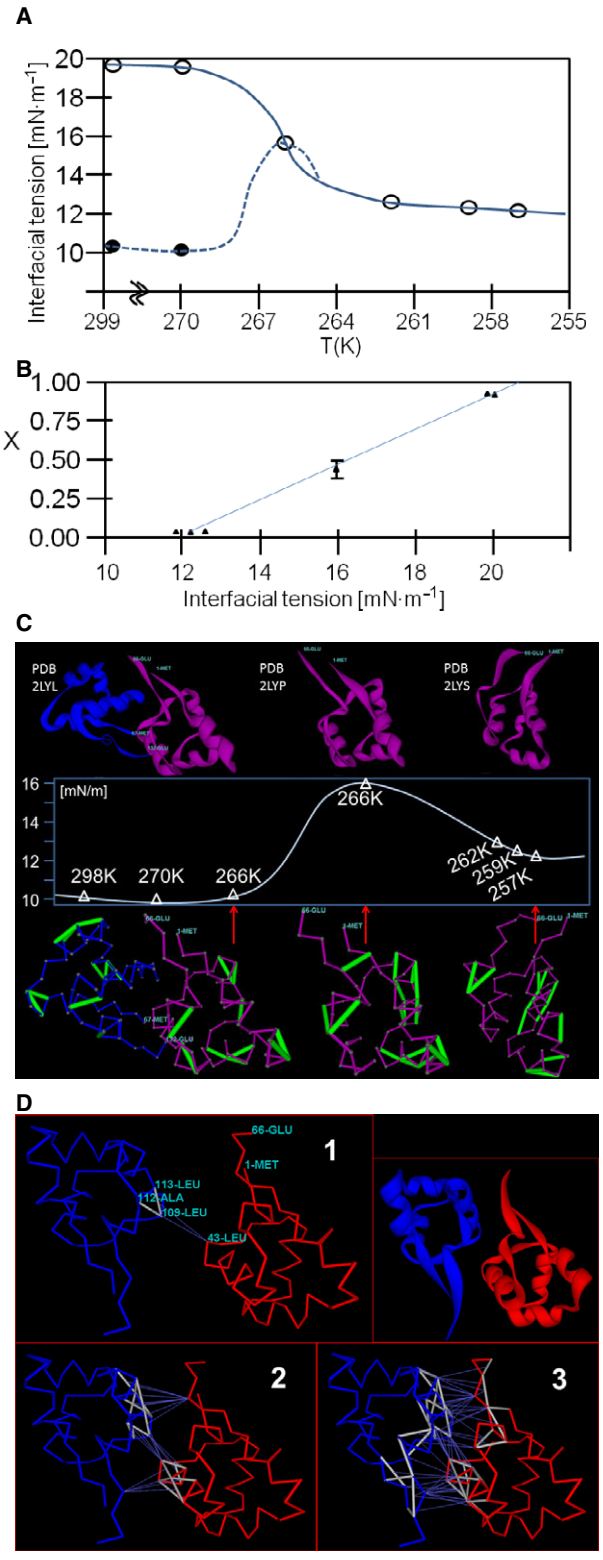

Fig. 4. Interfacial frustration and dimerization propensity of cold-denaturation intermediates of a protein complex: (A) Free-energy cost of interfacial frustration per unit surface area for the free monomeric subunit (open disks) and the subunit within the dimer (filled disks) for intermediate states resulting from progressive cold denaturation of the native homodimeric repressor protein CγIR2. The PDB files for the intermediates (absolute temperature in brackets) are 2LYJ (298 K), 2LYK (270 K), 2LYL (266 K, dimer), 2LYP (266 K, monomer), 2LYQ (262 K), 2LYR (259 K) and 2LYS (257 K). (B) Correlation between molar dimer/monomer ratio and free-energy cost of interfacial frustration per unit surface area for the free (uncomplexed) subunit in the cold-denaturation intermediates. (C) Hot spots of interfacial frustration (shown in green on the protein structure) for denaturation intermediate at 257 K (PDB 2LYS), and the inflexion-point intermediate with monomeric state in PDB 2LYP and dimeric state in PDB 2LYL. The inflexion-point intermediate is attributed two $\Delta G_{if}(\phi)$-values, one as free monomer and the other as subunit within the dimer. Hot spots are shown as solvent-exposed backbone hydrogen bonds or *dehydrons* (cf. Fig. 2). The chain conformation featuring hot-spot location is schematically represented by virtual bonds joining α-carbons. (D) Optimal frustration pathway leading to protein subunit association generated following the microstate sampling strategy in Methods (T = 298 K, computation time: 0.1 ms, number of iterations: 2–21 × 10^9). Initial conditions were provided by the structural coordinates of two dissociated CgIR2 subunits (PDB 2LYS). The chains are represented as virtual bonds joining α-carbons and intermolecular water exclusion from a PP interfacial dehydron is indicated by a line from the α-carbon of the approaching residue that promotes water removal to the center of the interfacial hydrogen bond. The latter are displayed as lines joining the α-carbons of the paired residues. Four runs reveal a unique nucleating configuration (1) at ~ 1 μs (±0.31 μs). Other reproducible configurations (2, 3) occur at ~ 19 μs and ~ 90 μs, with the latter (3 and ribbon representation) presenting the fully dehydrated PP interface with RMSD < 0.80 Å relative to the homodimer crystal in PDB entry 2LYJ.

[14]. Thus, the frustration-related interfacial tension is given in Fig. 4A for PDB entries (absolute temperatures in brackets) 2LYJ (298 K), 2LYK (270 K), 2LYL (266 K, dimer), 2LYP (266 K, monomer), 2LYQ (262 K), 2LYR (259 K), and 2LYS (257 K). The open disks correspond to the computation of interfacial tension = $\Delta G_{if}(\phi)/A$ for the free subunit with A = solvent-accessible surface area, while the filled disks represent the interfacial tension corresponding to one half of the $\Delta G_{if}(\phi)$-value for dimeric states, a valid estimation of the interfacial free-energy contribution for each subunit within a homodimer. It is clear that the inflexion point at 266 K represents a critically high interfacial tension beyond which the dimeric state prevails to mitigate the higher thermodynamic cost of spanning the interface as the temperature for complex renaturation is approached. A tight correlation (R^2 = 0.921, Fig. 4B) is obtained between dimer/monomer molar ratio X, a measure of association propensity obtained from average values of hydrodynamic radius [14], and the interfacial tension. This correlation validates the variational frustration

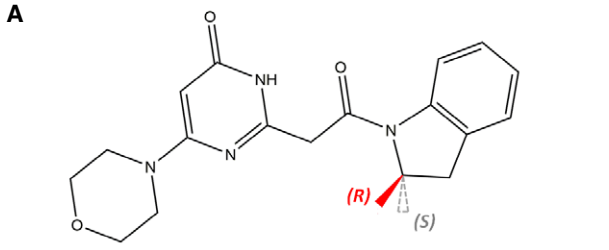

(*R*)-2-(2-(2-methylindolin-1-yl)-2-oxoethyl)-6-morpholinopyrimidin-4(3*H*)-one

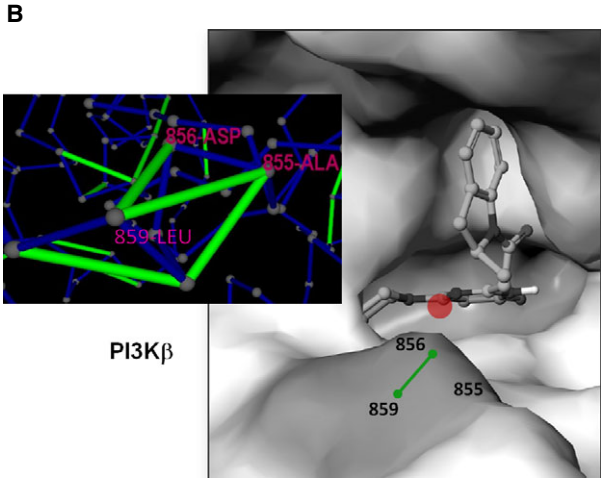

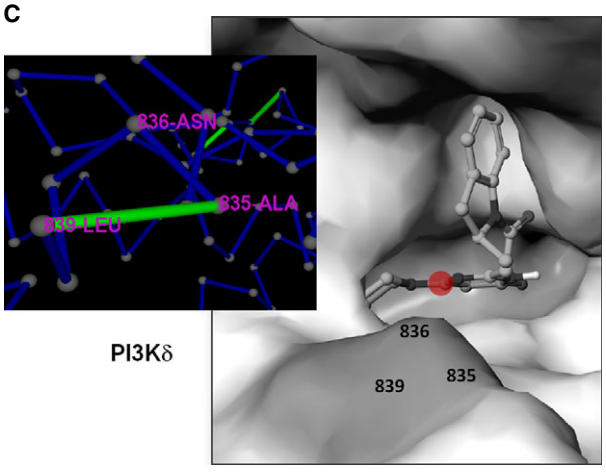

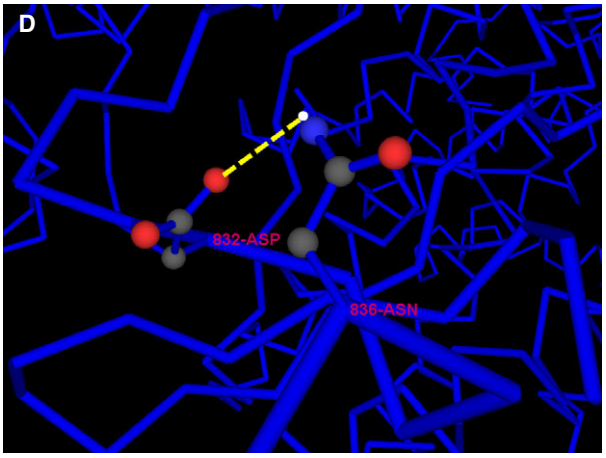

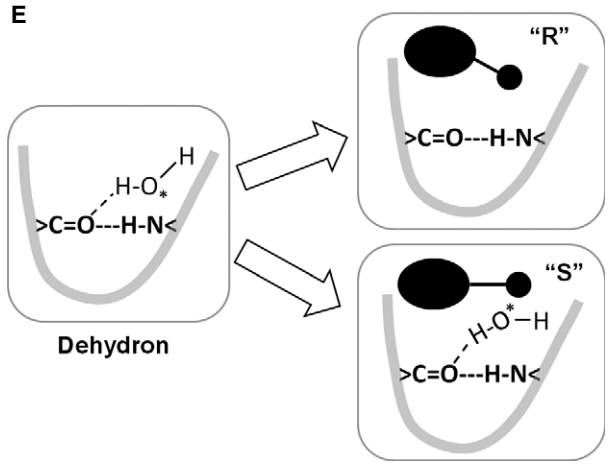

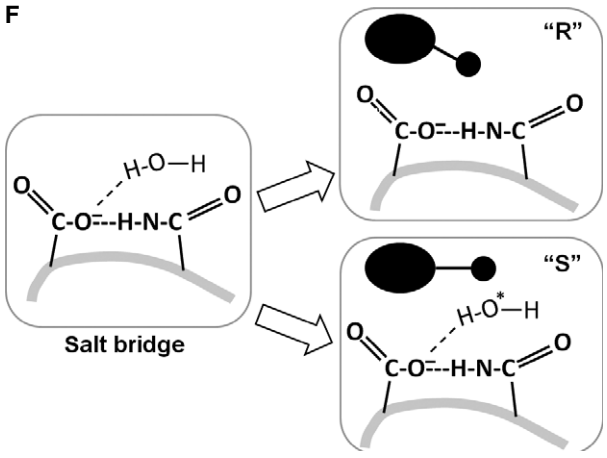

principle and its dynamic steering role in complex formation. The protein surface regions causative of interfacial frustration [5] are shown in green on Fig. 4C. Thus, hot spots in interfacial frustration (green, cf. Fig. 2) are shown for the most denatured intermediate (PDB 2LYS, 257 K), and the inflexion-point intermediate whose critically high interfacial frustration promotes significant dimerization at 266 K, with monomeric state in PDB 2LYP and dimeric state in PDB 2LYL. The inflexion-point intermediate is attributed two $\Delta G_{if}(\phi)$-values, one as free subunit (PDB 2YLP) and the other as subunit-within-dimer (PDB 2LYL).

Finally, the non-Debye frustration pathway leading to maximal reduction of interfacial tension conducive

Fig. 5. Drug design guided by the interfacial tension hot spots of the target protein: (A) Chemical structure of lead compound with nM affinity toward the β and δ-isoforms of PI3K. Two methylation substitutions intended to improve selectivity are shown: R-isomer in red, S-isomer in gray. The latter is predicted to endow the compound with discriminatory power, enhancing its selectivity toward the β-isoform. The R-isomer is named using IUPAC convention. (B) Hot spot of interfacial tension in drug-target PI3Kβ corresponding to dehydron Ala856–Leu859 (inset, PDB 4BFR). Dehydrons are displayed as green segments joining the α-carbons of residues paired by solvent-exposed backbone hydrogen bonds (cf. Fig. 2). The structure of the complex (panel with space-filling atoms) reveals that the S-isomer methylation shown in (A) targets dehydron Ala856–Leu859 with retention of hydrating molecule (red circle). The ligand binding does not appreciably increase the frustration of the water molecule that was already frustrated due to sub-nanoscale confinement within the dehydron cavity and re-accommodates upon binding to the S-ligand. (C) Dehydron pattern for PI3Kδ (PDB 4V0I). The Ala856–Leu859 dehydron in PI3Kβ aligns with backbone hydrogen bond Ala836–Leu839 in PI3Kδ, which is not solvent-exposed and hence does not cause significant water frustration ($\phi < 1$). This local difference in interfacial tension between PI3Kβ and PI3Kδ suggests the modifications featured in Fig. 1A as a means to enhance drug selectivity toward the β-isoform. (D) Salt bridge (dashed line) in PI3Kδ absent in PI3Kβ. (E) Scheme of frustration effects on dehydron-vicinal water upon binding the R- and S-isomer. Upon binding, the R-isomer excludes vicinal water, thus stabilizing the dehydron, while the S-isomer retains a water molecule but does not increase its frustration relative to the 'apo' form. The frustrated loner pair on the oxygen is marked by an asterisk. (F) Scheme of frustration effects on water vicinal to a salt bridge upon binding the R- and S-isomer. Upon binding, the R-isomer excludes vicinal water, thus stabilizing the salt bridge, while the S-isomer retains a water molecule significantly increasing its frustration relative to the 'apo' form.

to protein subunit association is generated following the flowchart (Fig. 1) in Methods at renaturation $T = 298$ K. We computed the path to minimally frustrated hydration adopting the structural coordinates of two fully dissociated CgIR2 subunits (PDB 2LYS) as initial condition. Four runs reveal a unique nucleating step at ~ 1 μs, ultimately leading to formation of the fully dehydrated PP interface. This step consists of intermolecular dehydration of dehydron Leu109–Ala112 and Leu109–Leu113 by Leu43 in the complementary binding subunit (Fig. 4D). The pathway leads to optimal mitigation of interfacial tension and ultimate formation of the dimer with RMSD < 0.80 Å relative to the homodimer crystal in PDB entry 2LYJ.

Discussion

The results presented reveal a protein 'epistructure' defined by the frustration state of the aqueous interface [5]. This concept is likely to impact drug design geared at impairing protein function through target–drug association whereby the interfacial tension of the target is reduced. As shown subsequently, such a design strategy is expected to enable an ultraselective control of the drug impact with discriminatory molecular recognition even at the level of isoforms of the target protein (> 80% sequence identity). Homologous proteins typically possess high structural similarity but the differences in composition translate into differences at the epistructural level which may be harness to design selective drugs that can tell them apart.

For example, it has been recognized that the phosphoinositide 3-kinase (PI3K) family is implicated in human cancer through its role in the regulation of diverse cellular processes [29]. Yet, pan-PI3K inhibitors that bind indiscriminately with nanomolar (nM) affinity to isoforms PI3K α, β, δ (class IA) are not desirable therapeutically due to off-target side effects [30]. It has become imperative to design drugs that can tell apart such isoforms. It would be desirable to re-engineering lead compounds to improve selectivity toward the β–isoform recognized as a crucial target in PTEN (phosphatase and tensin homolog)-deficient cancers [31]. In this regard, the lead compound *2-[2-(2,3-dihydro-indol-1-yl)-2-oxo-ethyl]-6-morpholin-4-yl-3H-pyrimidin-4-one* (Fig. 5A) binds with nM affinity to PI3K β and δ isoforms (IC_{50} = 4 and 28 nM, respectively) [31]. The specificity toward the β-isoform may be significantly enhanced by comparing the epistructures of both isoforms and modifying the lead compound to target epistructural differences (Fig. 5B,C). A first substitution (R-isomer, Fig. 5A) would in principle be suitable to selectively remove upon binding a preformed tension hot spot of interfacial tension present only in the β-isoform (cf. Fig. 5B,C). Indeed, there is an interfacial tension hot spot in drug target PI3Kβ corresponding to frustrated water partially hydrating dehydron Ala856–Leu859 (Fig. 5B). The crystal structure of the complex reveals that the methylation of the lead compound displayed in Fig. 5A targets dehydron Ala856–Leu859 upon drug–target association. However, the R-substitution does not endow the drug with higher discriminatory power toward the β-isoform [31]. This is *a priori* surprising because the Ala856–Leu859 dehydron in PI3Kβ aligns with solvent-shielded backbone hydrogen bond Ala836–Leu839 in PI3Kδ (Fig. 5B,C) which does not frustrate water nearby (cf. Fig. 2). The reason for the lack of specificity is that PI3Kδ features *in lieu* of a dehydron the exposed salt bridge Asp832–Asn836 (Fig. 5D) which gets dehydrated upon binding with the R-ligand, thereby becoming stabilized to an extent comparable to the dehydron [5]. The interfacial thermodynamics for ligand association reflect this observation, yielding

$\Delta\Delta G_{if}(\beta,\delta,R) \approx 0 \pm \frac{0.22kcal}{mol}$ for the difference in the interfacial free-energy change between the δ- and β- isoforms upon binding to the R-ligand. To achieve specificity one may instead *retain* the frustrated interfacial water molecule upon ligand binding, adopting the methylated S-ligand to that effect (Fig. 5B,C). In the respective apo-states, the $<\phi> = 1.7$ water frustration of water around dehydron 856–859 in the β-isoform becomes $<\phi> = 0.6$ for the water molecule closest to Asn836 in the δ-isoform. The resulting local difference in interfacial tension between PI3Kβ and PI3Kδ suggests adopting the S-ligand with retention of interfacial water upon binding, as shown in Fig. 5B,C in order to enhance specificity toward the β-isoform. Thus, the already frustrated water molecule around dehydron 856–859 simply rearranges to accommodate the S-ligand with $<\phi> = 1.7 \rightarrow <\phi> = 1.9$ upon binding, whereas the $<\phi> = 0.6$-water hydrating salt bridge Asp832–Asn836, becomes severely frustrated, with $<\phi> = 0.6 \rightarrow <\phi> = 1.8$, upon binding to the S-ligand (Fig. 5E,F). This trend is reflected in the thermodynamics: $\Delta\Delta G_{if}(\beta,\delta,S) \approx 2.8 \pm \frac{0.61\,kcal}{mol}$ indicative of a significantly higher affinity of the S-ligand toward the β-isoform. Experimental results uphold this prediction [31]. With $IC_{50} = 23$ and 468 nM for the β and δ-isoforms, respectively, the S-ligand is three times more selective toward PI3Kβ than the parental compound ($IC_{50} = 4$ and 28 nM, respectively).

This example illustrates the power of variational computations of frustrated hydration as a guide to design ultraselective drugs that could not be rationally conceived adopting standard structure-based approaches.

To reconcile thermodynamics and structural data on protein complexation, this work focused on the steering role of frustrated hydration in biomolecular associations. To make frustration at the aqueous interface amenable to variational methods, we introduced a 'frustration field' identifying locally unmet hydrogen-bonding opportunities due to sub-nanoscale confinement at each point in space. The frustration field was optimized variationally, and the dynamics resulting from the computational search were shown to drive protein associations with great specificity in order to mitigate frustration-related interfacial tension. Our computations entailed a microstate sampling method implemented to search for the state of minimal interfacial frustration within relaxation times for protein–water dynamic coupling. Spectroscopic measurements of dielectric relaxation upheld the basic tenets of the theory, while the crystallographic, affinity scanning and NMR record on protein assemblages attested to the validity of the minimal frustration principle.

The frustration model reported could be improved to deal with more realistic solvents reflective of physiological conditions in the cytosol. For example, ions in micromolar concentrations are likely to titrate surface charges on the protein surface or be engaged in coordination complexes that will affect the hydration patterns and interfacial frustration thereof.

The solvent-centric approach introduced in this work was shown to impact the design of ultraselective drugs, as it highlighted the targetable nature of the aqueous interface enabling the discrimination of closely related protein isoforms that could not be operationally distinguished using structure-based designs. In this regard, the role of dehydrons as selectivity filters has been recognized by this author [5] and others [32], yet the physical underpinnings of the concept are only provided in this paper.

Acknowledgements

The author is indebted to his former students at Rice University, Drs. Jianping Chen and Xi Zhang, for implementing the microstate sampling strategy on the Rice Computational Research Cluster.

Author contributions

AF performed all aspects of the research and wrote the paper.

References

1 Cheng YK and Rossky PJ (1998) Surface topography dependence of biomolecular hydrophobic hydration. *Nature* **392**, 696–699.
2 Wang L, Berne BJ and Friesner RA (2011) Ligand binding to protein binding pockets with wet and dry regions. *Proc Natl Acad Sci USA* **108**, 1326–1330.
3 Giovanbattista N, Lopez CF, Rossky PJ and Debenedetti PG (2008) Hydrophobicity of protein surfaces: separating geometry from chemistry. *Proc Natl Acad Sci USA* **105**, 2274–2279.
4 Snyder PW, Mecinović J, Moustakas DT, Thomas SW III, Harder M, Mack ET, Lockett MR, Héroux A, Sherman W and Whitesides GM (2011) Mechanism of hydrophobic effect in the biomolecular recognition of arylsulfonamides by carbonic anhydrase. *Proc Natl Acad Sci USA* **108**, 17889–17894.
5 Fernández Stigliano A (2015) Biomolecular Interfaces: Interactions, Functions and Drug Design, pp. 1–51. Springer, Berlin.

6 Fernández Stigliano A (2013) Breakdown of the Debye polarization ansatz at protein-water interfaces. *J Chem Phys* **138**, 225103.
7 Remsing RC, McKendry IG, Strongin DR, Klein ML and Zdilla MJ (2015) Frustrated solvation structures can enhance electron transfer rates. *J Phys Chem Lett* **6**, 4804–4808.
8 Lee M, Salsbury F and Olson MA (2004) An efficient hybrid explicit/implicit solvent method for biomolecular simulations. *J Comput Chem* **25**, 1967–1978.
9 Allen MP and Tildesley DJ (1989) Computer Simulation of Liquids. Clarendon Press, Oxford.
10 Bachmann M (2014) Thermodynamics and Statistical Mechanics of Macromolecular Systems. Cambridge University Press, Cambridge.
11 Lee MS and Olson MA (2013) Comparison of volume and surface area nonpolar solvation free energy terms for implicit solvent simulations. *J Chem Phys* **139**, 044119.
12 Fernández A (2011) Nanoscale thermodynamics of biological interfacial tension. *Proc R Soc A* **467**, 559–568.
13 Clackson T and Wells JA (1995) A hot spot of binding energy in a hormone-receptor interface. *Science* **267**, 383–386.
14 Jaremko M, Jaremko L, Kim H, Cho M, Schwieters C, Giller K, Becker S and Zweckstetter M (2013) Cold denaturation of a protein dimer monitored at atomic resolution. *Nat Chem Biol* **9**, 264–270.
15 Evans LC (2010) Partial Differential Equations. American Mathematical Society, Providence, RI.
16 Fernández A (2015) Quantum theory of interfacial tension quantitatively predicts spontaneous charging of nonpolar aqueous interfaces. *Phys Lett A* **379**, 2405–2408.
17 Pal SK, Peon J and Zewail AH (2002) Biological water at the protein surface: dynamical solvation probed directly with femtosecond resolution. *Proc Natl Acad Sci USA* **99**, 1763–1767.
18 Matsumoto M and Tanaka K (2008) Nano bubble – size dependence of surface tension and inside pressure. *Fluid Dyn Res* **40**, 546–553.
19 Li B, Liu P, Xu Z and Zhou S (2013) Ionic size effects: generalized Boltzmann distributions, counterion stratification and modified Debye length. *Nonlinearity* **26**, 2899–2922.
20 Jorgensen WL, Chandrasekhar J, Madura JD, Impey RW and Klein ML (1983) Comparison of simple potential functions for simulating liquid water. *J Chem Phys* **79**, 926–938.
21 Sierra MB, Accordino SR, Rodriguez-Fris A, Morini MA, Appignanesi GA and Fernández Stigliano A (2013) Protein packing defects "heat up" interfacial water. *Eur Phys J E* **36**, 62.
22 Wang J, Wolf RM, Caldwell JW, Kollman PA and Case DA (2004) Development and testing of a general amber force field. *J Comput Chem* **25**, 1157–1174.
23 Darden T, York D and Pedersen LJ (1993) Particle mesh Ewald: an N· log (N) method for Ewald sums in large systems. *J Chem Phys* **98**, 10089–10092.
24 Zhang L, Wang L, Kao Y, Qiu W, Yang Y, Okobiah O and Zhong D (2007) Mapping hydration dynamics around a protein surface. *Proc Natl Acad Sci USA* **104**, 18461–18466.
25 Ashkenazi A, Presta L, Marsters S, Camarato J, Rosenthal K, Fendly B and Capon D (1990) Mapping the CD4 binding site for human immunodeficiency virus by alanine-scanning mutagenesis. *Proc Natl Acad Sci USA* **87**, 7150–7154.
26 Castro MJ and Anderson S (1996) Alanine point-mutations in the reactive region of bovine pancreatic trypsin inhibitor: effects on the kinetics and thermodynamics of binding to beta-trypsin and alpha-chymotrypsin. *Biochemistry* **35**, 11435–11446.
27 Kuhlmann UC, Pommer A, Moore GR, James R and Kleanthous C (2000) Specificity in protein-protein interactions: the structural basis for dual recognition in endonuclease colicin-immunity protein complexes. *J Mol Biol* **301**, 1163–1178.
28 Bottger V, Bottger A, Garcia-Echeverria C, Chène P, Hochkeppel HK, Sampson W, Ang K, Howard SF, Picksley SM and Lane DP (1997) Molecular characterization of the hdm2-p53 interaction. *J Mol Biol* **269**, 744–756.
29 Maira SM, Voliva C and Garcia-Echeverria C (2008) Class IA phosphatidylinositol 3-kinase: from their biologic implication in human cancers to drug discovery. *Expert Opin Ther Targets* **12**, 223–238.
30 Ihle NT and Powis G (2010) The biological effects of isoform-specific PI3-kinase inhibition. *Curr Opin Drug Discov Devel* **13**, 41–49.
31 Certal V, Carry JC, Halley F, Virone-Oddos A, Thompson F, Filoche-Romme B, El-Ahmad Y, Karlsson A, Charrier V, Delorme C *et al*. (2014) Discovery and optimization of pyrimidone indoline amide PI3Kβ inhibitors for the treatment of phosphatase and tensin homologue (PTEN)-deficient cancers. *J Med Chem* **57**, 903–920.
32 Robinson DD, Sherman W and Farid R (2010) Understanding kinase selectivity through energetic analysis of binding site waters. *ChemMedChem* **5**, 618–627.

Supporting information

Additional Supporting Information may be found online in the supporting information tab for this article:

Appendix S1. Parameter estimation and experimental validation of equation (4).